

N- and p-type carrier injections into WSe₂ with van der Waals contacts of two-dimensional materials

Yohta Sata¹, Rai Moriya^{1,*}, Satoru Masubuchi¹, Kenji Watanabe², Takashi Taniguchi², and Tomoki Machida^{1,3,*}

¹*Institute of Industrial Science, The University of Tokyo, Meguro, Tokyo 153-8505, Japan*

²*National Institute for Materials Science, Tsukuba, Ibaraki 305-0044, Japan*

³*Institute for Nano Quantum Information Electronics, The University of Tokyo, Meguro, Tokyo 153-8505, Japan*

We demonstrated n-type and p-type carrier injections into a transition metal dichalcogenide (TMD) WSe₂ using van der Waals (vdW) contacts of two-dimensional (2D) materials: graphite for an n-type contact and NbSe₂ for a p-type contact. Instead of conventional methods such as the evaporation of metals on TMD, 2D metals were transferred onto WSe₂ in order to form van der Waals contacts. With these contacts, we demonstrated a small Schottky barrier height for both carrier polarities. Our finding reveals the potential of a high-performance vdW metal/semiconductor contact for use in electronics applications.

*E-mail: moriyar@iis.u-tokyo.ac.jp; tmachida@iis.u-tokyo.ac.jp

1.Introduction

Transition metal dichalcogenide (TMD) is extremely attractive for electronics and optoelectronics applications ¹⁻⁴⁾. In the bulk crystal, these materials have layered crystal structures; thus, individual layers have strong covalent bonding within the plane and different layers are vertically held together with van der Waals (vdW) interlayer force ⁵⁾. Because of the relatively weak vdW interaction, these materials can be easily exfoliated down to monolayer without having dangling bonds on the exfoliated surface. These unique TMD properties are highlighted for a wide variety of applications such as high-performance transistors ^{6,7)}, sensors ⁸⁾, flexible devices ⁹⁾, and photodetectors ^{10,11)}. However, the large contact resistance between metal and TMD seriously restricts the performance of these TMD-based devices ¹²⁾. In general, the material of the metal contact for TMD is selected in such a way that the bottom of the conduction band of TMD and the work function of the metal are aligned to form a Schottky-barrier-free n-type contact. In contrast, the contact can be of the p-type when the top of the valence band of TMD and the work function of the metal are aligned. Previous studies proved that the contact at metal/TMD interfaces was not solely determined by the position of the metal's work function with respect to the conduction or valence band of TMD ¹⁰⁾. It has been considered that there is an interface state at the evaporated metal/TMD interface. Because of the interface state, the Fermi level of the metals is pinned within the midgap of TMD, resulting in a large contact resistance at the evaporated metal/TMD interface. Instead of the evaporation of metals, the van der Waals contact between the two-dimensional (2D) metal and TMD has been drawing attention lately ^{13,14)}. Examples of 2D metals are graphene, 1T'-WTe₂, and 2H-NbSe₂, whereas conventional metals that are deposited by

thermal evaporation such as Au, Ti, and Pd are referred to as three-dimensional (3D) metals. Owing to the nonbonding nature of the vdW contact, it is expected that the interface state at the 2D metal/semiconducting TMD will be suppressed; thus, the surface pinning effect of the metal's Fermi level can be reduced. Moreover, since 2D metals have a wide variety of work functions, a significant reduction in contact resistance for both n- and p-type contacts for TMD is expected. A new method of forming contacts on TMD provides an opportunity to deepen our understanding of the properties of TMD. Here, we study the effect of a vdW contact between 2D metal/WSe₂ interfaces by fabricating field-effect transistor devices.

The work functions of 2D and conventional 3D metals are illustrated in Fig. 1(a). The positions of the conduction and valence bands of monolayer WSe₂ are shown together. The corresponding values are obtained from the recent density functional theory calculation results presented in Ref. 13. Various 2D metals with different work functions are also shown. The lowest and highest work functions of 2D metals are comparable to those of 3D metals. In our experiment, we selected graphite as a small-work-function material and NbSe₂ as a large-work-function material ^{15,16}. Regarding both materials, there were reports on their exfoliation down to monolayer and the fabrication of high-quality vdW heterostructures with other 2D materials ¹⁷⁻²⁸. Thus, they are suitable for forming n- and p-type contacts on WSe₂.

2. Device fabrication

The fabricated device structure and device micrograph are shown in Figs. 1(b)–1(e) for the graphite/WSe₂ [Figs. 1(b) and 1(d)] and NbSe₂/WSe₂ [Fig. 1(c) and 1(e)] devices.

Device fabrication was conducted by the one-by-one dry transfer of 2D materials in an atmospheric environment without any heating procedure^{27,29)}. First, hexagonal boron nitride (h-BN) with a thickness of 20–30 nm was mechanically exfoliated and deposited on a 300 nm SiO₂/doped-Si substrate. Second, few-layer WSe₂ was transferred to the flat surface of h-BN. Third, 3- to 6-nm-thick graphite or NbSe₂ layers were transferred. Finally, WSe₂ channels and part of the 2D metal contact were covered with another h-BN with a thickness of few nm to few tens of nm. The top and bottom h-BN layers served as the atomically flat substrate and encapsulation layer, respectively. These h-BN layers improved the uniformity of the WSe₂ layer and the adhesion between 2D metals and WSe₂ during transfer. The WSe₂ and NbSe₂ layers were exfoliated from bulk crystals (HQ Graphene Inc.). Graphite was exfoliated from Kish graphite. The electrical contacts for graphite and NbSe₂ were fabricated by the e-beam (EB) lithography and EB evaporation of 40 nm Au/40 nm Ti. The contact resistance of Au/Ti/graphite and Au/Ti/NbSe₂ junctions fabricated by this method was less than 1 k Ω and the junctions showed ohmic characteristics. The channel length L and channel width W of the devices were $W = 6.1\text{ }\mu\text{m}$ and $L = 5\text{ }\mu\text{m}$ for the graphite-contact device and $W = 3.5\text{ }\mu\text{m}$ and $L = 4.5\text{ }\mu\text{m}$ for the NbSe₂-contact device. The transport properties of the devices were measured in a variable-temperature cryostat from 240 to 300 K. Prior to the measurement, the devices were annealed for 6 h at 410 K within the cryostat. For transport measurements, the back-gate voltage V_{BG} was applied between the device and the doped-Si substrate to control the carrier density of the WSe₂ layer. The source-drain bias voltage V_{SD} was applied between the 2D metal contacts, and the source-drain current I flowing through the device was measured.

3. Results and discussion

The transport properties at room temperature for both the graphite/WSe₂/graphite and NbSe₂/WSe₂/NbSe₂ devices are shown in Figs. 2(a)–2(f). The V_{BG} dependence of the device current I measured under constant $V_{SD} = 50$ mV and 0.5 V, which are shown in Figs. 2(a) and (b), reveals distinct characteristics as follows. The graphite/WSe₂/graphite device exhibits a significantly higher current when the channel is electron-doped (positive V_{BG} region) than when it is hole-doped (negative V_{BG} region). In contrast, the NbSe₂/WSe₂/NbSe₂ device exhibits an opposite trend such that the current is higher when the WSe₂ channel is hole-doped than when it is electron-doped. From these comparisons, the graphite/WSe₂ vdW contact is preferred to be of the n-type, while the NbSe₂/WSe₂ vdW contact is preferred to be of the p-type. Since WSe₂ is exfoliated from the same batch of bulk crystal and the exfoliated flakes have nearly the same thickness, we think that the difference observed in Figs. 2(a) and 2(b) originates from the different carrier injection properties between graphite/WSe₂ and NbSe₂/WSe₂. We also note that the hysteresis between different V_{BG} sweep directions is small for both devices because of h-BN encapsulation³⁰; therefore, we think that the contamination of the WSe₂ surface caused by the adsorption of molecules could also be small for both devices. The current-voltage (I - V_{SD}) characteristics at $V_{BG} = +50$ V (-50 V) are presented for graphite/WSe₂/graphite [Fig. 2(c)] and NbSe₂/WSe₂/NbSe₂ [Fig. 2(e)]. The small nonlinearity observed in the I - V_{SD} curves suggests the small Schottky barrier at the 2D metal/WSe₂ junctions. The field-effect mobility of the devices is determined by the relation $\mu_{FE} = [L/(WC V_{SD})](dI/dV_{BG})$, where $C = \epsilon_0 \epsilon / d$ is the capacitance per unit area with the relative permittivity ϵ of 3.9 for both SiO₂ and h-BN, ϵ_0 being the vacuum permittivity

and d the thickness of the dielectrics. By differentiating I - V_{BG} curves, the mobilities for both devices are calculated at $V_{\text{SD}} = 0.6$ V and presented in Figs. 2(d) and 2(f). The carrier mobilities extracted by this method monotonically increase with V_{BG} , suggesting that the two-terminal transport of each device is limited by the contact resistance at 2D metal/WSe₂ rather than by the channel resistance of WSe₂. Generally, the change in contact resistance with V_{BG} induces a nonlinear I - V_{BG} curve; thus, the mobilities are not constant with respect to V_{BG} . The significance of contact resistance could be inferred from the shift of the threshold voltage of the device shown in Figs. 2(a) and 2(b), which depends on V_{SD} . The nonlinearity in the I - V_{SD} curve, which appeared in Figs. 2(c) and 2(e), also supports this speculation. Nevertheless, as a reference, we extracted the maximum electron mobility $\mu_e = 18 \text{ cm}^2\text{V}^{-1}\text{s}^{-1}$ for the graphite/WSe₂/graphite device and maximum hole mobility $\mu_h = 17 \text{ cm}^2\text{V}^{-1}\text{s}^{-1}$ for the NbSe₂/WSe₂/NbSe₂ device. With the assumption that the two-terminal transports of the devices are fully dominated by their contact resistance, we estimated the contact resistance of the devices using the following sequence. First, the drain current I at $V_{\text{SD}} = +0.6$ V was measured at $V_{\text{BG}} = +50$ V for the graphite/WSe₂/graphite device and at $V_{\text{BG}} = -50$ V for the NbSe₂/WSe₂/NbSe₂ device. V_{SD}/I was nearly equal to the contact resistance $2R_c$. Then, R_c was multiplied by its contact width W . We obtained $R_c W = 780 \text{ k}\Omega\mu\text{m}$ for the graphite/WSe₂ contact and $R_c W = 540 \text{ k}\Omega\mu\text{m}$ for the NbSe₂/WSe₂ contact.

Next, to evaluate the Schottky barrier height between 2D metal and WSe₂, the temperature dependence of the I - V_{BG} curve at $V_{\text{SD}} = 0.1$ V was measured and the results are plotted in Fig. 3(a) for the graphite-contact device and in Fig. 3(d) for the NbSe₂-contact device. The lower the temperature, the lower the conductance in both devices;

this suggests that the thermionic emission across the metal/TMD interface is a dominant transport mechanism. These data were analyzed on the basis of the thermionic emission theory such that

$$I = A^* T^2 \exp\left(-\frac{e\phi_B}{k_B T}\right) \left[\exp\left(-\frac{eV_B}{k_B T}\right) + 1 \right], \quad (1)$$

where A^* represents the effective Richardson constant, ϕ_B the barrier height at the metal/WSe₂ interface, e the elementary charge, k_B the Boltzmann constant, and T the temperature. By making the Arrhenius plot, the measured data is fitted with Eq. (1) and the derived barrier height ϕ_B is plotted against V_{BG} as shown in Figs. 3(b) and 3(e). ϕ_B changes with V_{BG} according to the gate modulation of the carrier density in the WSe₂ layer. There are particular ϕ_B values indicated by arrows in Figs. 3(b) and 3(e); above these values, ϕ_B changes linearly with respect to V_{BG} , reflecting thermionic transport, while below them, both thermionic and tunneling transport processes are reflected. It is generally known that these particular ϕ_B values give the Schottky barrier height ϕ_{SB} at a metal/TMD interface³¹⁾. From these analysis results, we obtained ϕ_{SB} values of 63 meV between the Fermi level of graphite and the conduction band edge of WSe₂ [(Fig. 3(c)] and 50 meV between the Fermi level of NbSe₂ and the valence band edge of WSe₂ [Fig. 3(f)]. Since the surface pinning effect at a 3D metal/WSe₂ interface pins the metal's Fermi level at 0.2–0.3 eV above the valence band¹⁰⁾, the demonstration of the n-type contact for WSe₂ with graphite suggests that the vdW contact is not restricted by the pinning effect. The obtained Schottky barrier height between graphite and WSe₂ is comparable to that obtained at a low resistance 3D metal/MoS₂ contact; it ranges from 20 to 100 meV¹⁰⁾. Here, we compared our observation with the result of the 3D metal/MoS₂ contact since

MoS₂ is more widely used for the n-type TMD transistor. Therefore, our finding suggests the potential advantage of using the graphite/WSe₂/graphite structure for n-type transistors. Notably, the p-type Schottky barrier height that we achieved in the NbSe₂/WSe₂ junction is significantly smaller than the typical values for a 3D metal/WSe₂ interface, which range from 0.27 to 0.45 eV¹⁰⁾. Furthermore, such a junction is superior to recently reported NbSe₂/W_xNb_{1-x}Se₂/WSe₂ vdW heterojunctions fabricated from CVD-grown TMD crystals^{28,32)}. We believe that our mechanical exfoliation of CVT-grown NbSe₂ and encapsulation with h-BN crystals provide a higher quality NbSe₂/WSe₂ vdW interface; thus, these methods enable us to achieve a smaller Schottky barrier height.

Our experimental results reveal the control between the n- and p-type contacts with a 2D metal/WSe₂ vdW heterostructure. This suggests that the vdW contact is not seriously restricted by the Fermi level pinning effect. However, the obtained Schottky barrier heights at graphite/WSe₂ and NbSe₂/WSe₂ are different from the theoretically calculated energy alignment presented in Fig. 1(a). From Fig. 1(a), it is expected that the graphite/WSe₂ junction will behave as an ambipolar contact with a large Schottky barrier height for both carriers, and that the NbSe₂/WSe₂ junction will behave as a p-type contact without a barrier. We note that the conduction and valence band positions of WSe₂ shown in Fig. 1(a) are calculated in the monolayer case, not the few-layer WSe₂ used in our experiment. However, the difference in band gap between the few-layer WSe₂ and the monolayer WSe₂ is ~0.2 eV^{33,34)}, which is too small to explain the discrepancy. By using the band gap of the few-layer WSe₂ ($E_g \sim 1.40$ eV)^{33,34)} and the obtained band offset at the graphite/WSe₂ and NbSe₂/WSe₂ interfaces in our experiment, the work function difference between graphite and NbSe₂ is calculated as ~1.29 eV. This difference in work

function is close to the theoretical difference of 1.30 eV [Fig. 1(a)]. Therefore, we think that, by shifting the relative energy between WSe₂ and 2D metal, our experimental results and theoretical calculations exhibit a better agreement. It has been considered that interlayer coupling at a vdW junction alters the relative energy alignment between WSe₂ and metal^{35,36}; this could explain our observation. More detailed comparisons between experimental and theoretical results by fabricating a series of 2D metal/TMD vdW junctions with different 2D metals are necessary in future experiments.

4. Conclusions

We demonstrated n- and p-type carrier injections into WSe₂ using vdW contacts between WSe₂ and 2D metals: graphite for an n-type contact and NbSe₂ for a p-type contact. The fabrication of n- and p-type transistors based on the same channel material could be suitable for circuit applications. This finding supports the concept of utilizing a vdW metal/semiconductor contact superior to those used in conventional methods.

Acknowledgements

This work was supported by CREST, Japan Science and Technology Agency (JST) and JSPS KAKENHI Grant Numbers JP25107003, JP25107004, JP26248061, JP15H01010, and JP16H00982.

Figure captions

Fig. 1.

(Color online)(a) The theoretically calculated work functions of monolayer 2D and 3D metals are plotted together with the positions of the bottom of the conduction band and the top of the valence band of monolayer WSe₂. Their values were obtained from Ref. 13. (b, c) Structures of (b) graphite/WSe₂/graphite and (c) NbSe₂/WSe₂/NbSe₂ devices. (d, e) Optical microscopy images of (d) graphite/WSe₂/graphite and (e) NbSe₂/WSe₂/NbSe₂ devices.

Fig. 2.

(Color online) (a, b) $I-V_{BG}$ relationship of (a) graphite/WSe₂/graphite and (b) NbSe₂/WSe₂/NbSe₂ devices. The data measured in different V_{BG} sweep directions are plotted. (c, e) $I-V_{SD}$ curves of (c) graphite/WSe₂/graphite ($V_{BG} = +50$ V) and (e) NbSe₂/WSe₂/NbSe₂ ($V_{BG} = -50$ V) devices. (d, f) V_{BG} dependence of the carrier mobility in (d) graphite/WSe₂/graphite and (f) NbSe₂/WSe₂/NbSe₂ devices.

Fig. 3.

(Color online) (a, d) Temperature dependence of $I-V_{BG}$ curves of (a) graphite/WSe₂/graphite and (d) NbSe₂/WSe₂/NbSe₂ devices measured from 300 to 240 K ($V_{SD} = 0.1$ V). (b, e) V_{BG} dependence of the Schottky barrier height at (b) graphite/WSe₂ and (e) NbSe₂/WSe₂ junctions. (c, f) Illustration of obtained band offset at (c) graphite/WSe₂ and (f) NbSe₂/WSe₂ junctions.

References

- 1) F. Xia, H. Wang, D. Xiao, M. Dubey, and A. Ramasubramaniam: *Nat. Photonics* **8**, 899 (2014).
- 2) G. Fiori, F. Bonaccorso, G. Iannaccone, T. Palacios, D. Neumaier, A. Seabaugh, S. K. Banerjee, and L. Colombo: *Nat. Nanotechnol.* **9**, 768 (2014).
- 3) K. F. Mak and J. Shan: *Nat. Photonics* **10**, 216 (2016).
- 4) Z. Sun, A. Martinez, and F. Wang: *Nat. Photonics* **10**, 227 (2016).
- 5) A. K. Geim and I. V. Grigorieva: *Nature* **499**, 419 (2013).
- 6) Y. Yoon, K. Ganapathi, and S. Salahuddin: *Nano Lett.* **11**, 3768 (2011).
- 7) M. Chhowalla, D. Jena, and H. Zhang: *Nat. Rev. Mater.* **1**, 16052 (2016).
- 8) S. J. Heerema and C. Dekker: *Nat. Nanotechnol.* **11**, 127 (2016).
- 9) D. Akinwande, N. Petrone, and J. Hone: *Nat. Commun.* **5**, 5678 (2014).
- 10) Y. Liu, N. O. Weiss, X. Duan, H.-C. Cheng, Y. Huang, and X. Duan: *Nat. Rev. Mater.* **1**, 16042 (2016).
- 11) F. H. L. Koppens, T. Mueller, P. Avouris, A. C. Ferrari, M. S. Vitiello, and M. Polini: *Nat. Nanotechnol.* **9**, 780 (2014).
- 12) A. Allain, J. Kang, K. Banerjee, and A. Kis: *Nat. Mater.* **14**, 1195 (2015).
- 13) Y. Liu, P. Stradins, and S.-H. Wei: *Sci. Adv.* **2**, e1600069 (2016).
- 14) M. Farmanbar and G. Brocks: *Adv. Electron. Mater.* **2**, 1500405 (2016).
- 15) T. Shimada, F. S. Ohuchi, and B. A. Parkinson: *Jpn. J. Appl. Phys.* **33**, 2696 (1994).
- 16) T. Takahashi, H. Tokailin, and T. Sagawa: *Phys. Rev. B* **32**, 8317 (1985).
- 17) X. Cui, G.-H. Lee, Y. D. Kim, G. Arefe, P. Y. Huang, C.-H. Lee, D. A. Chenet, X. Zhang, L. Wang, F. Ye, F. Pizzocchero, B. S. Jessen, K. Watanabe, T. Taniguchi, D. A. Muller, T. Low, P. Kim, and J. Hone: *Nat. Nanotechnol.* **10**, 534 (2015).
- 18) Y. Liu, H. Wu, H.-C. Cheng, S. Yang, E. Zhu, Q. He, M. Ding, D. Li, J. Guo, N. O. Weiss, Y. Huang, and X. Duan: *Nano Lett.* **15**, 3030 (2015).
- 19) W. J. Yu, Z. Li, H. Zhou, Y. Chen, Y. Wang, Y. Huang, and X. Duan: *Nat. Mater.* **12**, 246 (2013).
- 20) T. Georgiou, R. Jalil, B. D. Belle, L. Britnell, R. V. Gorbachev, S. V. Morozov, Y.-J. Kim, A. Gholinia, S. J. Haigh, O. Makarovskiy, L. Eaves, L. A. Ponomarenko, A. K. Geim, K. S. Novoselov, and A. Mishchenko: *Nat. Nanotechnol.* **8**, 100 (2013).
- 21) R. Moriya, T. Yamaguchi, Y. Inoue, S. Morikawa, Y. Sata, S. Masubuchi, and T. Machida: *Appl. Phys. Lett.* **105**, 083119 (2014).
- 22) T. Yamaguchi, R. Moriya, Y. Inoue, S. Morikawa, S. Masubuchi, K. Watanabe, T. Taniguchi, and T. Machida: *Appl. Phys. Lett.* **105**, 223109 (2014).
- 23) Y. Sata, R. Moriya, T. Yamaguchi, Y. Inoue, S. Morikawa, N. Yabuki, S. Masubuchi, and T. Machida: *Jpn. J. Appl. Phys.* **54**, 04DJ04 (2015).
- 24) Y. Sata, R. Moriya, S. Morikawa, N. Yabuki, S. Masubuchi, and T. Machida: *Appl. Phys. Lett.* **107**, 023109 (2015).
- 25) R. Moriya, T. Yamaguchi, Y. Inoue, Y. Sata, S. Morikawa, S. Masubuchi, and T. Machida: *Appl. Phys. Lett.* **106**, 223103 (2015).
- 26) D. K. Efetov, L. Wang, C. Handschin, K. B. Efetov, J. Shuang, R. Cava, T. Taniguchi, K. Watanabe, J. Hone, C. R. Dean, and P. Kim: *Nat. Phys.* **12**, 328 (2016).

- 27) N. Yabuki, R. Moriya, M. Arai, Y. Sata, S. Morikawa, S. Masubuchi, and T. Machida: *Nat. Commun.* **7**, 10616 (2016).
- 28) A. R. Kim, Y. Kim, J. Nam, H.-S. Chung, D. J. Kim, J.-D. Kwon, S. W. Park, J. Park, S. Y. Choi, B. H. Lee, J. H. Park, K. H. Lee, D.-H. Kim, S. M. Choi, P. M. Ajayan, M. G. Hahm, and B. Cho: *Nano Lett.* **16**, 1890 (2016).
- 29) A. Castellanos-Gomez, M. Buscema, R. Molenaar, V. Singh, L. Janssen, H. S. J. van der Zant, and G. A. Steele: *2D Mater.* **1**, 011002 (2014).
- 30) G.-H. Lee, X. Cui, Y. D. Kim, G. Arefe, X. Zhang, C.-H. Lee, F. Ye, K. Watanabe, T. Taniguchi, P. Kim, and J. Hone: *ACS Nano* **9**, 7019 (2015).
- 31) S. Das, H.-Y. Chen, A. V. Penumatcha, and J. Appenzeller: *Nano Lett.* **13**, 100 (2013).
- 32) Y. Kim, A. R. Kim, J. H. Yang, K. E. Chang, J.-D. Kwon, S. Y. Choi, J. Park, K. E. Lee, D.-H. Kim, S. M. Choi, K. H. Lee, B. H. Lee, M. G. Hahm, and B. Cho: *Nano Lett.* **16**, 5928 (2016).
- 33) K. Kim, S. Larentis, B. Fallahazad, K. Lee, J. Xue, D. C. Dillen, C. M. Corbet, and E. Tutuc: *ACS Nano* **9**, 4527 (2015).
- 34) K. Liu, L. Zhang, T. Cao, C. Jin, D. Qiu, Q. Zhou, A. Zettl, P. Yang, S. G. Louie, and F. Wang: *Nat. Commun.* **5**, 4966 (2014).
- 35) J. Kang, W. Liu, D. Sarkar, D. Jena, and K. Banerjee: *Phys. Rev. X* **4**, 031005 (2014).
- 36) Y. Wang, R. X. Yang, R. Quhe, H. Zhong, L. Cong, M. Ye, Z. Ni, Z. Song, J. Yang, J. Shi, J. Li, and J. Lu: *Nanoscale* **8**, 1179 (2016).

Figure 1

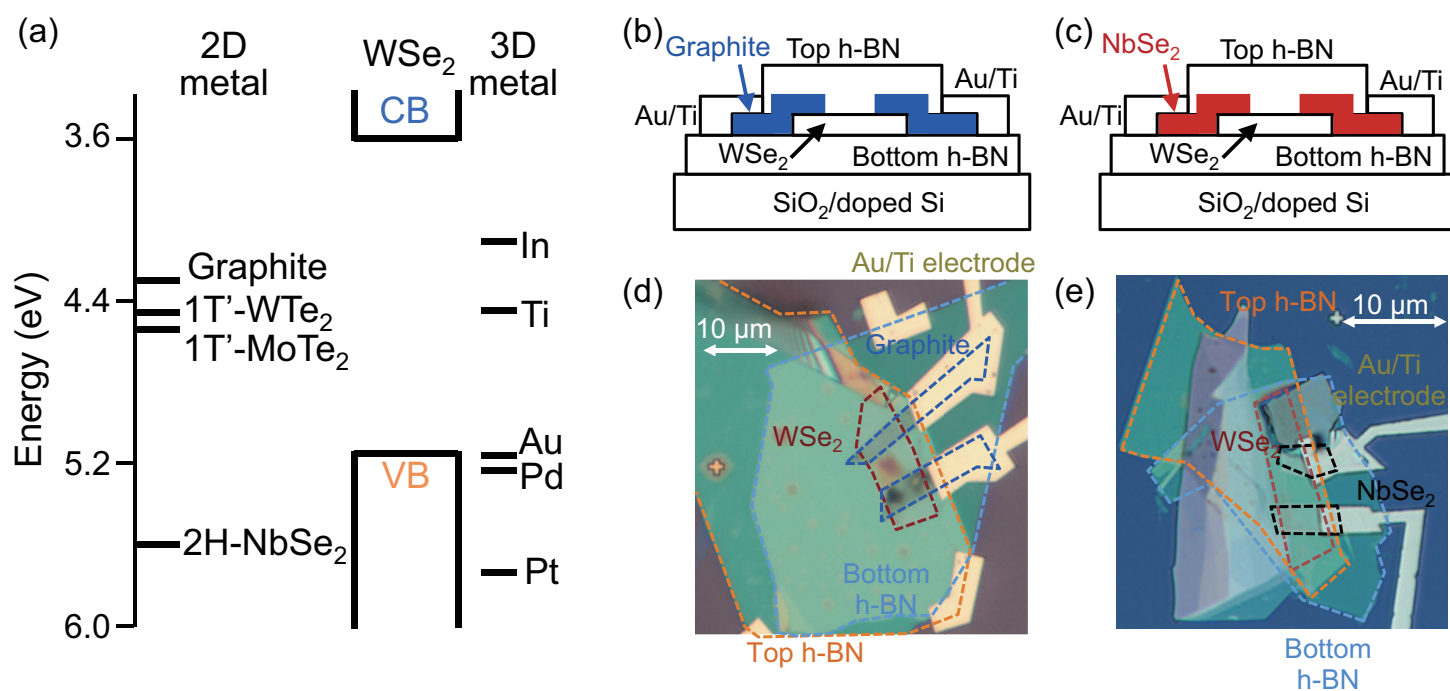


Figure 2

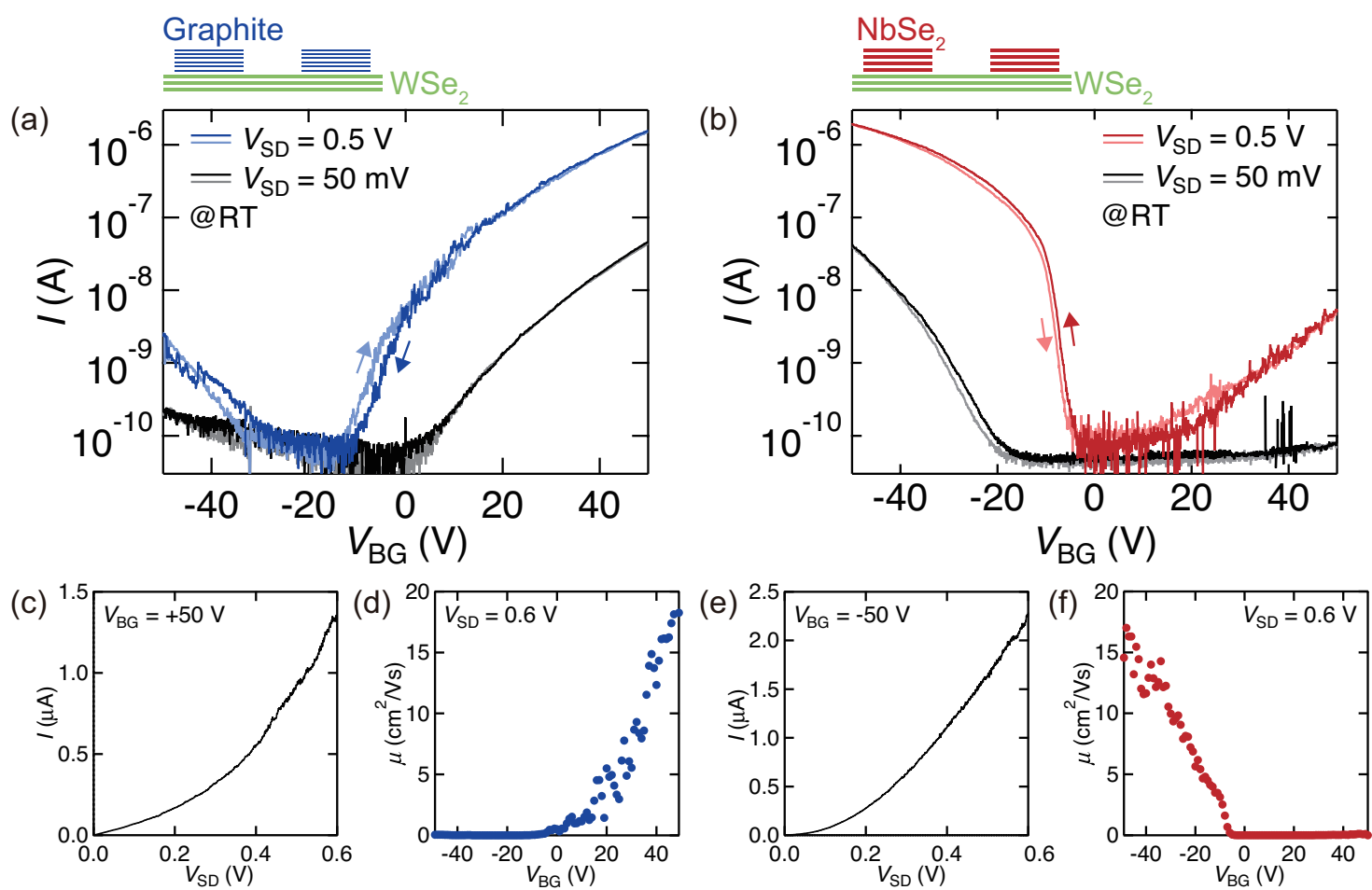


Figure 3

